

Distillation Improves Visual Place Recognition for Low Quality Images

Anbang Yang^{*}, Ge Jin^{*}, Junjie Huang, Yao Wang, John-Ross Rizzo, Chen Feng[✉]

Abstract—Real-time visual localization often utilizes online computing, for which query images or videos are transmitted to remote servers for visual place recognition (VPR). However, limited network bandwidth necessitates image-quality reduction and thus the degradation of global image descriptors, reducing VPR accuracy. We address this issue at the descriptor extraction level with a knowledge-distillation methodology that learns feature representations from high-quality images to extract more discriminative descriptors from low-quality images. Our approach includes the Inter-channel Correlation Knowledge Distillation (ICKD) loss, Mean Squared Error (MSE) loss, and Triplet loss. We validate the proposed losses on multiple VPR methods and datasets subjected to JPEG compression, resolution reduction, and video quantization. We obtain significant improvements in VPR recall rates under all three tested modalities of lowered image quality. Furthermore, we fill a gap in VPR literature on video-based data and its influence on VPR performance. This work contributes to more reliable place recognition in resource-constrained environments. Source code and data available at <https://github.com/ai4ce/LoQI-VPR>.

I. INTRODUCTION

Visual Place Recognition (VPR) has rapidly become a foundational component in machine perception. By condensing RGB images into compact vector representations, devices can recognize previously visited locations and recall their locations through only vision input and an image database of known locations [1, 2]. VPR has become a critical component in applications ranging from robots navigating complex industrial settings to augmented reality systems overlaying digital data onto the physical world to wayfinding applications that support vulnerable populations [3, 4, 5].

The adaptability of VPR to diverse environments has expanded its use cases. From smartphones to autonomous vehicles, the need for efficient and precise VPR systems is rising. However, this demand, especially in consumer devices, introduces novel challenges. A primary concern is the rapid growth in scene diversity and volume for real-world VPR applications, leading to large image databases that pose storage challenges for devices with limited capacity [6, 7].

Furthermore, the goal of more precise image descriptor vectors and thus better VPR performance has led to more complex VPR methods [8, 9, 10]. While such advancements do not delay descriptor matching, they increase the computational demands of extracting descriptors from images.

^{*} Equal contribution.

New York University, Brooklyn, NY 11201, USA

[✉] Corresponding author (cfeng@nyu.edu). This work is supported partly by NSF Grants 2238968 and 2345139; by the National Eye Institute and Fogarty International Center under Grants R21EY033689, R33EY033689, and R01EY036667; and by the NYU IT High Performance Computing resources, services, and staff expertise.

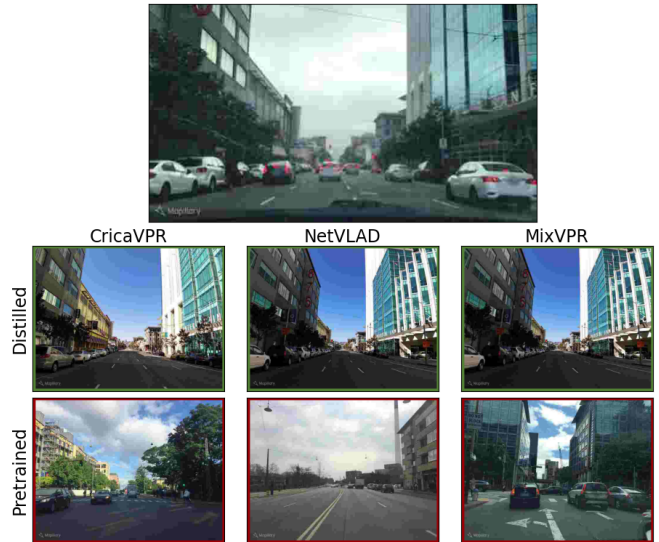


Fig. 1: **Enhanced Low Quality Image Retrieval:** After knowledge distillation from high quality images, multiple VPR methods succeeds in their VPR recall of this JPEG-compressed query image from the Mapillary SLS dataset, while the same methods fail to do so beforehand.

Thus, real-time VPR on standard devices becomes more challenging due to significant computational cost [11] in addition to storage needs.

Transitioning to online computation, where images are transmitted over the network for centralized processing, could be a solution for both issues but not without difficulties. While many devices simultaneously capture images to query the VPR image database, real-time communication with servers becomes a bottleneck. As most real-world VPR applications localizes over image sequences, the underlying video streaming service could alleviate network bandwidth pressure through reducing resolution and increasing compression of images and quantization of video streams. However, these measures degrade image descriptors and reduce localization accuracy [12].

For this online VPR paradigm, we propose a VPR-specific knowledge-distillation framework that improves descriptor generation and thus VPR performance under low-quality images, offering the following contributions:

- We develop a strategy to distill state-of-the-art VPR methods’ knowledge of high-quality images into that of low-quality images, significantly improving performance on low-quality images.
- We demonstrate three distillation loss functions on multiple public datasets and analyze the nature of each

on descriptor quality.

- We validate the generalizability of our approach by extending it to multiple forms of image quality reduction, including resolution decrease and video quantization, curating a video-based VPR dataset in the process to also fill a gap in video data for VPR research.

II. RELATED WORK

A. VPR’s Challenges with Low-Quality Images

Prevailing VPR literature frames the problem of image-based localization as an image retrieval task [2]. Under this modality, VPR performance is heavily dependent on image descriptors’ abilities to relate images with distinct appearances to geographical proximity. Earlier VPR techniques such as GIST [13], HOG [14], and VLAD [15] generate compact image descriptors through hand-crafted local feature extractors. For better image matching performance, NetVLAD [8] and other recent VPR methods such as Patch-NetVLAD [16], MixVPR [9], AnyLoc [10], DINOv2 SALAD [17], Bag-of-Queries [18], and CrlicaVPR [19] leverage progress in deep learning and utilize convolutional and attention-based neural networks to produce learned local features and extract global image-level descriptors.

However, the rising complexity of VPR global descriptor extraction, while improving image retrieval accuracy, poses computational challenges, particularly in resource-constrained devices across real-world applications. Although special-purpose VPR techniques [11, 20, 21] with low computational cost address this limitation, the transmission of images for centralized descriptor extraction is often still necessary for deploying VPR techniques at scale [22, 23], completely free of both storage and computational constraints. Nevertheless, the resulting decrease in image quality from networking limitations reduces localization accuracy, which occurs under both lowered image resolution [12] and increased JPEG compression [24]. As many existing VPR datasets consist of purely JPEG images [25, 26, 27, 28, 29, 30, 31, 32, 33], the JPEG format’s prevalence both in VPR and in general [34] makes JPEG compression a main avenue of image quality reduction, besides decreasing image resolution. To our best knowledge, there exists a gap in VPR literature on publicly available datasets offering video data, and the effects of video quantization on VPR performance remain largely unexplored.

B. Knowledge Distillation and Transfer Learning in VPR

Likewise, research on effective methods to extract more representative global descriptors from low-quality images is also lacking in the VPR community. Existing solutions have addressed the issue at the descriptor matching and image-retrieval level. The authors of [24] propose a sequence-based image-retrieval strategy [35], which queries the database images multiple times with lower per-query cost thanks to JPEG compression. Furthermore, predicting the retrieval success for each query image could favor points within the sequential queries that are more easily localized [36]. We instead wish to explore knowledge distillation as a means to

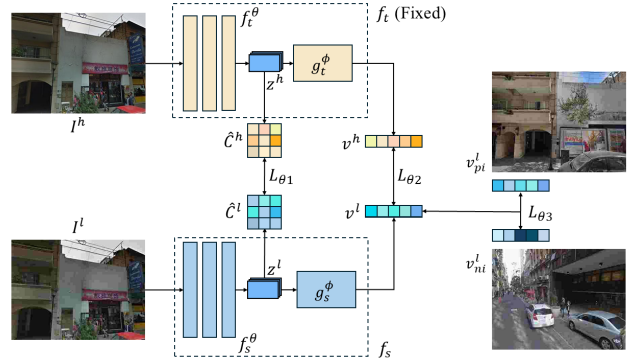


Fig. 2: **Proposed Knowledge Distillation Methodology:** Through ICKD loss between latent codes z^h and z^l , MSE loss between global descriptors v^h and v^l , and triplet loss on v^l , the student branch f_s learns the teacher branch f_t ’s knowledge of high quality images I^h to extract more discriminative, representative v^l from low quality images I^l .

directly improve descriptor extraction and thus increase the accuracy of database retrieval via individual queries.

After knowledge distillation was first proposed in [37], it has been applied to various computer-vision tasks such as super-resolution [38], image classification [39, 40], and segmentation [40]. More recently, knowledge distillation has also been used specifically in VPR to produce more discriminative global descriptors, such as learning from structural knowledge of an image-segmentation model [41]. We believe that knowledge distillation could similarly improve VPR accuracy for low-quality images.

III. DISTILLATION METHODOLOGY

Our goal was to enhance existing VPR methods to extract more representative global descriptors when given lower-quality images. Thus, we apply knowledge distillation techniques at the descriptor extraction level of VPR. For any VPR method, we aim to allow a student descriptor extractor handling low-quality images to approximate the output of its teacher counterpart, handling high-quality images.

Conceptual Model of Distillation for VPR

Given some VPR method, we initialize it twice to form the teacher branch f_t and student branch f_s , processing high-quality image I^h and its low-quality counterpart I^l respectively. As illustrated by fig. 2, we conceptualize the teacher model as consisting of a feature encoder f_t^θ and descriptor aggregator g_t^ϕ . Likewise, the student consists of a structurally identical encoder f_s^θ and aggregator g_s^ϕ . Between the encoder and aggregator, the student and teacher branch generates 3D latent code z^l and z^h , respectively. Finally, both branches aggregate their latent codes into global descriptors v^l and v^h . Our distillation methodology has three loss functions that operate on this understanding of VPR methods.

ICKD Loss

The Inter-Channel Correlation Knowledge Distillation (ICKD) loss [40] operates on the latent codes z^l and z^h . Given the potential size differences between inputs I^l and

I^h , the latent codes z^l and z^h may differ in dimensions. Traditional distillation losses, which typically require matching dimensions for the latent codes, are not directly applicable. Instead, the ICKD loss computes a standard-size Inter-Channel Correlation (ICC) matrix for both f_s^θ and f_t^θ , allowing the former to approximate the latter.

To illustrate ICKD loss, define I^l with resolution $W \times H$ and let the dimensions of their latent codes z^h and z^l be $c \times W' \times H'$ and $c \times w' \times h'$, respectively. Leveraging c being fixed, the ICKD concatenates along the remaining dimensions w' and h' to produce vector p^l with dimensions $c \times w' \cdot h'$. p^l is then normalized along its second dimension, producing $\hat{p}^l = \frac{p^l}{\|p^l\|}$. The subsequent ICC matrix $C^l = \hat{p}^l \times \hat{p}^{lT}$ with dimensions $c \times c$ is normalized to $\hat{C}^l = \frac{C^l}{\|C^l\|}$. A similar procedure for z^h yields $\hat{C}^h \in \mathbb{R}^{c \times c}$. The ICKD loss, formulated to ensure f_s^θ learns from f_t^θ , is defined as:

$$L_{\theta 1} = \|\hat{C}^l - \hat{C}^h\|_2. \quad (1)$$

Mean Squared Error (MSE) Loss

In addition to comparing latent codes, we directly compute the discrepancies between the image descriptors v^l and v^h . The MSE loss is expressed as:

$$L_{\theta 2} = \|v^l - v^h\|_2^2. \quad (2)$$

The MSE loss trains f_s to produce similar global descriptors as f_t despite different input images, gaining insights from f_t by directly emulating f_t 's outputs [42].

Weakly Supervised Triplet Ranking Loss

Applied exclusively within the student branch f_s , this loss is inspired by NetVLAD [8]. It ensures that the input image's descriptor v^l is more similar to that of a geographically proximate (positive) image, $\{v_p^l\}$, than that of a distant (negative) image, $\{v_n^l\}$. The goal is to satisfy the inequality $d_\theta(v^l, v_p^l) < d_\theta(v^l, v_n^l)$, where d_θ denotes the Euclidean distance between descriptors.

The triplet loss is articulated as:

$$L_{\theta 3} = \sum_j l \left(\min_i d_\theta^2(v^l, v_{p_i}^l) - d_\theta^2(v^l, v_{n_j}^l) + m \right). \quad (3)$$

In this equation, l represents the hinge loss, defined as $l(x) = \max(x, 0)$. The term m is a margin parameter, ensuring a buffer between positive and negative pairs, thereby enhancing the discriminative capabilities of the learned embeddings. The component $\min_i d_\theta^2(v^l, v_{p_i}^l)$ selects the descriptor of the most similar image as estimated by the student model f_s , ensuring the loss is attuned to the nearest matches.

Composite Loss

We also aim to assess the effectiveness of a combined loss function relative to the individual application of the aforementioned losses. We compute a cumulative loss as:

$$L = L_{\theta 1} + \alpha L_{\theta 2} + \beta L_{\theta 3}. \quad (4)$$

In this equation, α and β are weighting coefficients for $L_{\theta 2}$ and $L_{\theta 3}$, balancing the influence of each loss within the

composite function. Our experiments will also examine each loss's individual effects on distillation.

IV. EXPERIMENTAL SETUP

To analyze the efficacy of $L_{\theta 1}$, $L_{\theta 2}$, $L_{\theta 3}$, and L , we performed distillation on the student branch f_s using the GSV-Cities VPR dataset [32]. Afterwards, we evaluated f_s 's retrieval accuracy via the Deep Visual Geo-localization Benchmark [43] and some of its available testing datasets. For the following training and testing datasets, we define low quality images I^l as their original images (I^h) after 90% JPEG compression (quality level = 10).

Following Tomita et al. [35], we evaluate f_s with I^l VPR database and queries to avoid arbitrarily hampering descriptor matching from inconsistent compression levels, which also confirms the advantage of decreased database building cost when expecting I^l queries. Here, we reduce image quality via JPEG compression due to the absence of video data and other image formats. We would explore our methodology's generalizability to low image resolution and high video quantization in section VI.

A. Datasets Configurations

1) *Training Dataset:* The GSV-Cities dataset contains approximately 530,000 street view images of cities around the world collected from various years. The 23 total cities in the dataset are divided into a higher and lower resolution group containing images at 640×480 and 400×300 . To decrease training cost, we designated only the cities with lower resolution images to be used, effectively shrinking the dataset to approximately 194,000 images. This selective use of GSV-Cities additionally investigates whether knowledge distillation could be successful without high quality training data in the absolute sense.

TABLE I: Image Count of Testing Datasets

Partition	Mapillary SLS	Nordland	Tokyo 24/7
Database	18871	27592	75984
Queries	11084	2760	315

2) *Testing Datasets:* We tested f_s after distillation using each loss combination by calculating its VPR recall rate on three VPR datasets organized using VPR Datasets Downloader, namely Mapillary SLS [29], Nordland [26], and Tokyo 24/7 [28]. For each dataset, we follow the designated test partition and its database and query image specifications. Additional context for each dataset is provided below:

- Mapillary SLS is specifically curated for lifelong VPR featuring images from 30 cities.
- Nordland is created with forward-facing recordings across four seasons from trains along a rail route. Our version of the dataset is sourced identically as [9].
- Tokyo 24/7 depicts urban scenes at different times of day within Tokyo's Shibuya ward.

TABLE II: **Best Performance of VPR Methods after Distillation:** For low quality images, the loss combination producing the highest recall rate is compared against the baseline of fine-tuning. For both distilled and fine-tuned weights, the change in VPR recall is represented as a delta relative to the performance of each method using pretrained weights. Within each dataset and method, **greene** text indicates the greatest improvement for every R@N, whereas any decrease relative to pretrained performance is marked as **red**. The recall rates using pretrained weights on unmodified I^h images are provided as reference.

VPR Methods	Configuration	Mapillary SLS				Nordland				Tokyo 24/7			
		R@1	R@2	R@5	R@10	R@1	R@2	R@5	R@10	R@1	R@2	R@5	R@10
MixVPR	pretrained (I^h)	82.73	86.67	89.73	91.65	57.79	64.13	71.49	76.41	87.30	89.52	92.06	93.65
	pretrained (I^l)	71.87	76.61	81.22	84.19	31.05	36.12	44.13	51.23	66.03	73.33	78.73	82.22
	finetuned	+4.43	+3.86	+3.60	+2.99	+13.37	+14.28	+14.64	+14.46	+9.52	+7.62	+6.03	+5.40
	ICKD	+4.33	+3.69	+3.20	+2.93	+15.00	+16.59	+16.78	+15.94	+8.25	+6.03	+6.35	+6.67
CricaVPR	pretrained (I^h)	74.74	80.92	86.09	88.75	87.64	90.65	94.24	95.80	90.16	92.38	95.56	96.19
	pretrained (I^l)	68.14	74.41	80.24	83.19	63.51	69.71	77.46	82.64	74.29	79.68	84.76	87.94
	finetuned	-0.12	-0.64	-0.77	-0.23	-2.97	-2.93	-2.97	-2.79	+5.08	+4.44	+2.54	+1.90
	ICKD	+0.89	+1.39	+1.11	+1.14	+11.63	+10.80	+8.95	+7.03	+6.98	+5.08	+6.03	+4.76
DINOv2 SALAD	pretrained (I^h)	89.20	92.40	94.70	95.84	88.08	90.94	94.13	95.98	97.14	97.46	98.73	99.05
	pretrained (I^l)	84.60	88.85	91.89	93.68	67.90	73.88	80.40	84.24	89.21	92.06	95.87	96.51
	finetuned	-0.22	-0.57	-0.60	-0.76	+0.04	-0.40	-0.76	-0.04	-0.63	0.00	-0.95	0.00
	ICKD	+0.52	+0.45	+0.20	+0.30	+1.56	+1.81	+1.09	+1.20	+1.59	+1.27	+0.32	0.00
NetVLAD	pretrained (I^h)	49.29	55.24	62.07	67.29	5.51	6.67	8.62	11.38	60.63	63.81	69.21	74.29
	pretrained (I^l)	32.60	37.67	44.92	50.13	1.99	3.01	4.93	7.07	27.94	33.02	41.90	47.94
	finetuned	+0.03	+0.01	-0.02	-0.01	0.00	0.00	0.00	0.00	0.00	0.00	0.00	0.00
	MSE	+4.46	+5.32	+5.09	+5.01	+0.54	+0.43	-0.18	-0.72	+8.25	+6.35	+6.03	+5.08
AnyLoc	pretrained (I^h)	56.51	62.31	68.28	72.89	12.90	16.23	20.18	24.28	88.25	91.11	94.92	96.83
	pretrained (I^l)	48.04	56.45	63.84	69.17	10.11	12.97	17.86	21.92	83.49	87.30	91.75	95.87
	ICKD + Triplet	+0.99	+1.54	+2.68	+2.44	+1.74	+1.88	+1.52	+2.54	-5.71	-1.59	+1.59	-0.95

B. VPR Methods

To validate the applicability of knowledge distillation for VPR, we carried out the aforementioned experiments on five VPR methods from various points in the VPR literature, namely NetVLAD [8], MixVPR [9], AnyLoc [10], DINOv2SALAD [17], and CricaVPR [19]. While the former two methods have CNN backbones, the remaining methods are based on DINOv2 [44]. The diverse architectures of these five methods allow us to explore our distillation approach’s applicability to diverse VPR methodologies. Furthermore, to study each loss component’s effects on f_s ’s performance, we trained f_s under each of the seven possible combinations of L_{θ_1} , L_{θ_2} , and L_{θ_3} , using at least one term from (4). For each VPR method, we acquire pretrained model weights released with their public source codes to act as f_t and initialize f_s for faster training convergence.

As a baseline to be compared against distillation, we also fine-tune all methods except for AnyLoc using their unmodified training source code on the same I^l and pretrained weights as distillation. Given that AnyLoc uses off-the-shelf DINOv2 backbone and does not learn its aggregator weights, we only apply distillation to this method.

C. Experimental Setup

1) *Training Configuration:* We set the loss weighting coefficients in (4) to $\alpha = 10^5$ and $\beta = 10^4$. The learning rate is initialized at 10^{-5} , modulated by a decay factor of 2×10^{-11} , and further adjusted by an exponential rate of 0.99999. Each training experiment (ie. one of seven loss combinations with one of five methods) consists of one complete iteration through the shrunken GSV-Cities dataset

IV-A.1 (ie. one epoch). For the triplet loss (3), we sampled 5 negative images to form v_n^l for each training image.

2) *VPR Performance Evaluation:* To assess f_s ’s VPR performance after distillation, we use the metric Recall at N (referred to as R@N) found in [7, 8, 9, 10, 16, 17, 19] to calculate f_s ’s recall rate, which measures the percentage of successfully localized query images. Given a choice of N , a query to the VPR database is deemed successful if one of the top N retrieved database images is within d meters of the query’s true position for some predetermined threshold d . The percentage of successfully retrieved query images becomes f_s ’s R@N score for that N . In our evaluation procedures, we selected N values of 1, 2, 5, and 10, whereas d remained fixed at 25 meters following the distance thresholds used by the VPR methods we experimented with.

V. RESULTS AND DISCUSSIONS

For each loss combination, We use f_s after distillation to generate v^l for the selected testing datasets IV-A.2. We then calculate recall rates for different versions of f_s and analyze the efficacy of each configuration of our proposed distillation methodology.

A. Quantitative Results

Table II demonstrates the applicability of (4) and its components to a representative selection of VPR methods and datasets. Albeit with varying magnitudes, the deltas of recall rates under v^l after distillation and those under v^l from pretrained weights are generally positive. However, fine-tuning is inconsistent and mostly less effective than distillation. The Nordland recall rates for MixVPR and CricaVPR,

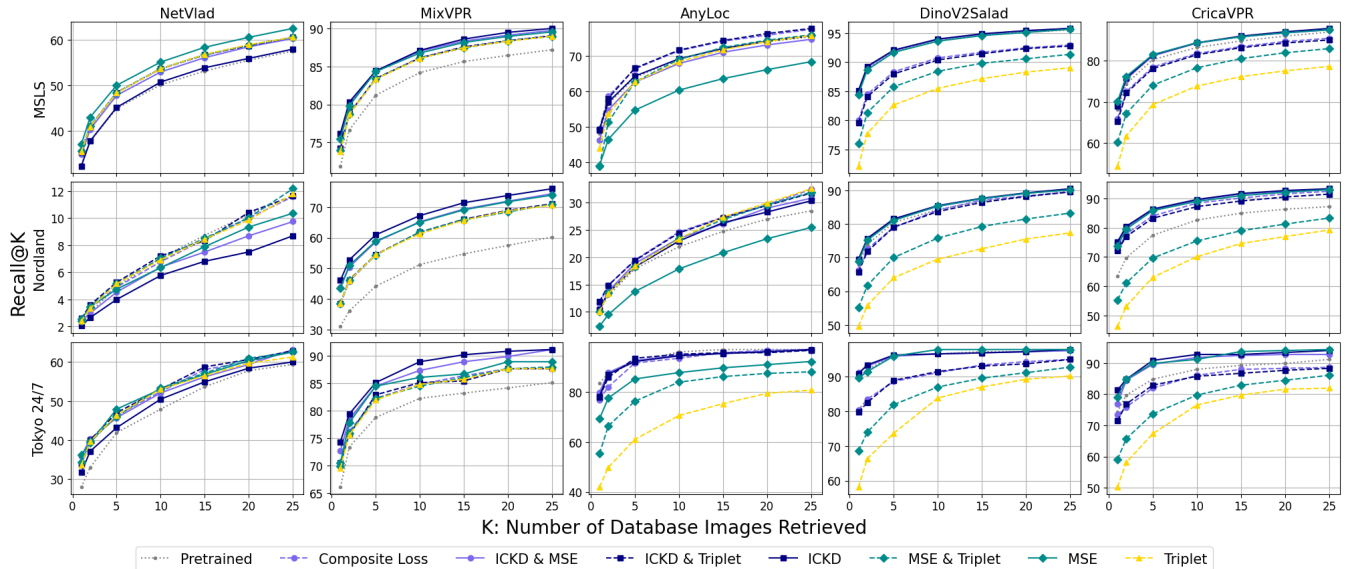


Fig. 3: **Recall Rates for All Losses:** For each method, we compare f_s after distillation with loss combinations as well as pretrained weights. Different marker shapes indicate different combinations of ICKD and MSE losses, whereas including the triplet loss is shown with a dashed line. For readability, the y-axis of each subplot is independently scaled.

two architecturally distinct methods, exemplifies distillation’s superior efficacy and applicability. There are only two instances where distillation partially failed to increase VPR recall rates under v^l for some method and dataset, namely NetVLAD on Nordland and AnyLoc on Tokyo 24/7. As AnyLoc’s recall rates fluctuate greatly on Tokyo 24/7, we postulate the combination of the natures of this method and dataset to be an edge case. Since NetVLAD’s improvement on Nordland for all R@N is less than that on other datasets, we reserve this phenomenon for further analysis in V-B.

Besides numerically demonstrating the most effective distillation losses, we graphically compare each loss combination in fig. 3, where we analyze full recall rate data for all variants of f_s . Previously, we have observed that ICKD (1) produces best VPR performances for MixVPR and CricaVPR and that MSE (2) is best for NetVLAD, and these three methods benefit the most from distillation. Now, the relative superiority of the two aforementioned losses could be seen on all methods, where the recall rates for f_s trained under either or both of them generally trend towards the top of all loss combinations. Here, AnyLoc and NetVLAD on Nordland are exceptions, where augmenting (1) or (2) with triplet loss (3) produces a better-performing f_s . However, besides NetVLAD, whose original training scheme uses the triplet loss, (3) is generally the least effective when used alone.

B. Qualitative results

We further investigate distillation’s effects on MixVPR, CricaVPR, and NetVLAD, the most improved methods, and potentially account for the latter’s more limited improvement on Nordland. In fig. 4, we plot activation maps for each method’s encoder f_s^θ after distillation with their respective best-performing loss. From each of the three VPR testing datasets IV-A.2, we visualize an I^l query where f_s improves

TABLE III: Indoor Evaluation Using Pretrained Weights

Methods	Quality	TUM LSI		Gangnam Station		NYC-Indoor-VPR	
		R@1	R@5	R@1	R@5	R@1	R@5
MixVPR	I^h	94.09	99.55	4.39	13.63	41.23	83.76
	90%	91.36	99.09	3.93	11.76	40.04	80.76
CricaVPR	I^h	92.27	99.09	7.48	21.64	37.92	82.36
	90%	92.27	97.27	7.67	21.37	37.30	79.26
DINOv2 SALAD	I^h	94.09	99.09	8.93	22.67	39.89	82.98
	90%	91.82	98.64	9.43	21.37	39.58	81.69
NetVLAD	I^h	95.00	99.09	3.21	8.36	39.42	81.27
	90%	91.82	98.18	2.94	9.81	38.23	79.10
AnyLoc	I^h	97.73	99.55	4.47	12.79	37.92	82.77
	90%	93.64	98.18	3.63	11.11	36.37	81.07

upon f_t . On Mapillary SLS and Nordland, distillation mitigates the distraction of uninformative sky features especially for NetVLAD and MixVPR. More generally, distillation shifts focus from repetitive foreground features, such as road surfaces and ground-level vegetation, to more structurally distinct whole-scene features, such as the contours of buildings and farther tree lines. In the case of NetVLAD, the highly selective focus of f_s^θ could account for its lesser recall rate improvement on Nordland. For the other two methods, while MixVPR’s improvement could be more intuitively attributed to increased overall focus on informative image regions, CricaVPR’s comparatively smaller change in focus suggests that its improvements originates from other factors, possibly concerning its aggregator g_s^ϕ .

VI. ADDITIONAL EXPERIMENTS

While our knowledge distillation approach already demonstrates notable efficacy for the majority of methods and datasets tested, we extend distillation to more datasets and other aforementioned routes of image quality reduction II-A.

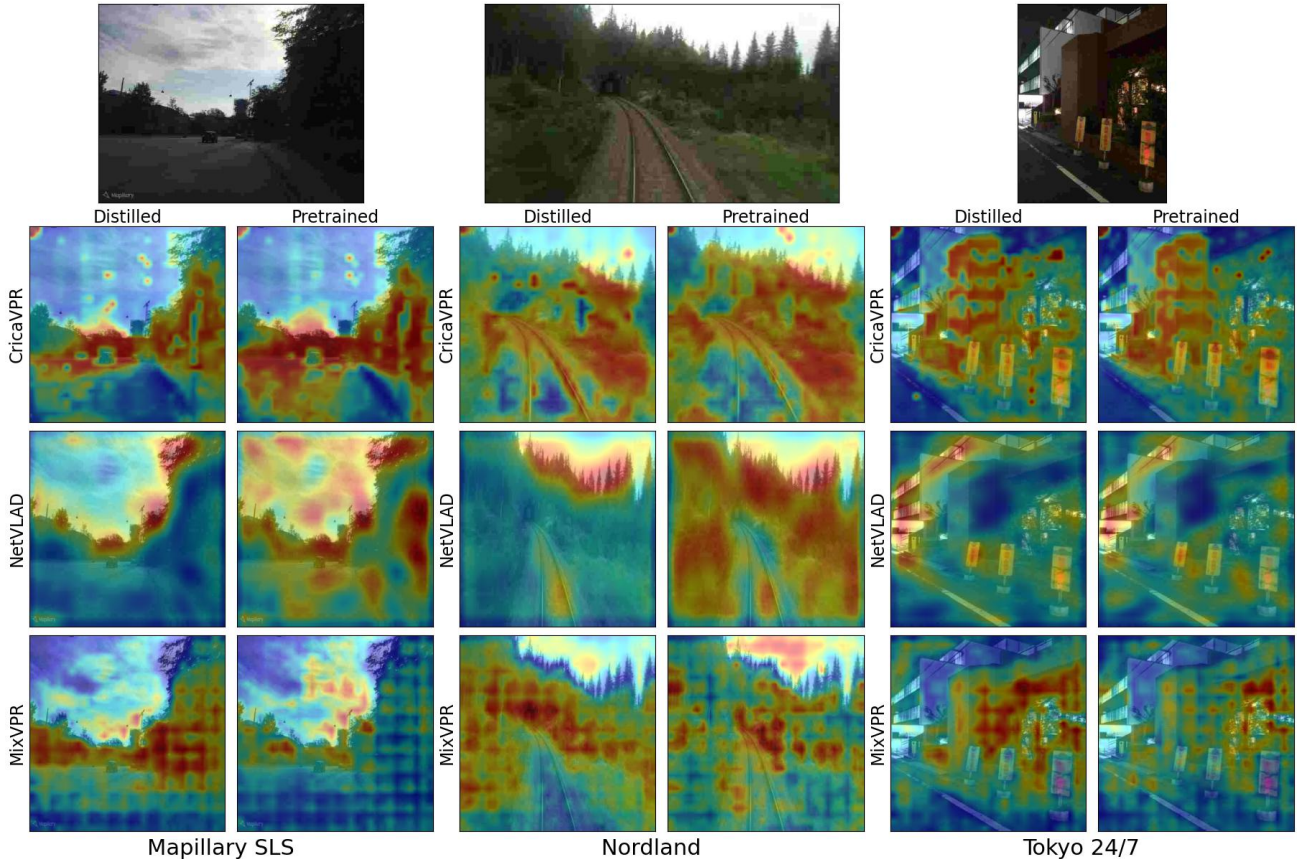


Fig. 4: **Activation Maps:** The selected I^l queries (top of figure) are successfully recalled by f_s , while f_t fails. For CricaVPR, the focus of its ICKD-trained f_s is visualized by averaging its z^l across the channel dimension in accordance with its authors. For NetVLAD, we averaged a weighted sum of its MSE-trained z^l via tentative cluster assignments from g_s^ϕ . For MixVPR, since its authors did not visualize activations, we masked small regions of I^l and considered the resulting change in its ICKD-trained v_l as activations, creating block-like patches on its heatmap.

A. JPEG Compression’s Impacts on Indoor Datasets

While our previous VPR testing datasets cover both rural and urban environments and contain temporal changes and perceptual aliasing, they all capture outdoor environments. In table III, We further examine the impacts of JPEG compression on three indoor datasets of different difficult levels, namely TUM LSI [27], Gangnam Station (one of NAVER LABS’ large-scale localization datasets [30]), and NYC-Indoor-VPR [33]. While the performance of all methods with pretrained weights fluctuate greatly across datasets, JPEG compression’s impacts on recall rates are significantly smaller than previous results with outdoor datasets. We postulate that due to indoor environments generally lack large contiguous regions of uninformative features such as sky, the proportion of distinctive features degraded by JPEG compression is smaller within indoor images. Therefore, instead of repeating our previous experiments, we extend our distillation methodology to other possible forms of I^l .

B. Other Modalities of Image Quality Reduction

Inferring from JPEG compression’s greater impacts on outdoor scenes, we use outdoor datasets from IV-A.2 to yield

I^l with reduced resolution instead of JPEG compression. Secondly, we explore the impacts of video quantization on VPR recall, mirroring realistic practice of streaming image data through video. However, the image-based nature of existing VPR datasets prompts us to curate a custom video-based VPR dataset to produce I^l with increased video quantization.

Amongst the five methods in table II, NetVLAD suffers the most from lowered image quality in general. Thus, we select NetVLAD as the candidate of verifying knowledge distillation’s benefits for VPR performance under resolution and quantization-based I^l .

C. Custom Video-Based VPR Dataset

Our custom VPR dataset is sourced from indoor spaces of the 6th floor of the Lighthouse Guild, an eye care facility in New York City. Instead of following existing indoor VPR datasets in capturing images [27, 30, 31, 33], we record panoramic videos using the Insta360 camera, providing a 360° view. Each frame, with dimensions 5760 × 2880, was horizontally segmented into 18 perspective images with 90° field of view and dimensions 1440 × 810. These images

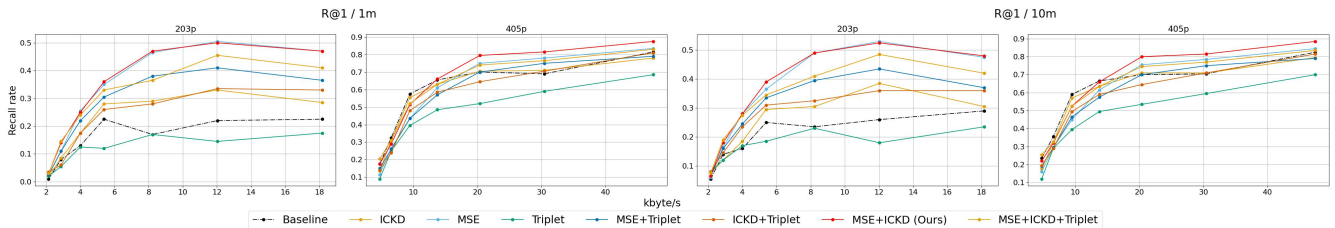


Fig. 5: **Results on Our Dataset:** The recall rates of Pitts250k-trained f_s are obtained for each quantization parameter. For ease of visualization, the latter is converted into the video bitrate metric with lower bitrate indicating higher quantization. The left two plots were calculated with a VPR threshold of 1m, and the right two have a 10m threshold.

were assembled into perspective videos for both resolution reduction and video quantization according to the following:

- Resolutions: 405p (720×405), 203p (360×203)
- Quantization Parameters: 30, 33, 36, 39, 42, 45, 48

D. Resolution and Quantization Experimental Results

We not only validate distillation’s efficacy for different forms of I^l but also its independence to datasets and I^l ’s modality during training. While following IV-C.1’s steps, we perform distillation on NetVLAD using the Pitts250k dataset [25], which contains around 250,000 outdoor 640×480 images of Pittsburgh’s urban environments. All images are reduced to 240×180 as I^l for f_s to learn on. To analyze distillation’s robustness to changing I^l modalities, we test NetVLAD’s recall on our custom dataset with v^l extracted from resolutions of 405p and 203p and quantization parameters spanning from 30 to 48 in intervals of 3. For previous outdoor datasets, we extract v^l from 320×240 (240p). The influence of our dataset’s various resolutions and quantization levels on f_s ’s recall rate after distillation is compared against pretrained weights as a baseline in Fig. 5. The 203p results restate MSE (2)’s efficacy on NetVLAD, but despite ICKD (1)’s comparatively inferior performance on constant-modality I^l before, combining the two losses further improves VPR performance on 405p, suggesting ICKD’s greater adaptability under video quantization. Notably, changing recall distance thresholds as defined in IV-C.2 has little effect on VPR performance.

For outdoor datasets, we compare pretrained NetVLAD against trained f_s with the highest recall rate in table IV. NetVLAD’s best-performing distillation loss remains MSE, but the addition of ICKD yields stronger performance on Tokyo 24/7. This corroborates the previous observation of ICKD’s adaptability, which may allow f_s to better withstand changing I^l modalities from 180p during distillation to 240p in testing.

VII. CONCLUSION

Addressing the concern of reduced VPR accuracy under the realistic scenario of image quality reduction, our knowledge distillation methodology for extracting more discriminative descriptors from low quality images achieves significant performance gains under JPEG and video compression for various VPR methods and datasets. Furthermore, we have demonstrated our approach’s potential to generalize to other

TABLE IV: NetVLAD’s Performance on 240p Images

Dataset	Configuration	R@1	R@2	R@5	R@10
Mapillary SLS	pretrained	31.16	37.89	46.36	52.54
	MSE	+7.57	+7.88	+7.64	+7.54
Nordland	pretrained	3.99	5.40	8.34	10.40
	MSE	+1.12	+1.23	+1.23	+1.81
Tokyo 24/7	pretrained	24.84	29.62	39.49	48.41
	ICKD + MSE	+7.64	+8.28	+7.64	+7.32

kinds of low quality images such as low resolutions, reducing the literature gap on video-based VPR datasets in the process.

A suitable direction of **future work** is to justify distillation’s effects on different kinds of VPR methods. While we have identified the general strengths of ICKD and MSE losses and noted the specific usability of the triplet loss, a better understanding of each VPR method’s affinity to specific losses could reveal further insights on VPR methods themselves. Secondly, more VPR datasets and research under the context of video quantization could prove valuable for the future real-world applications of VPR.

ACKNOWLEDGMENT

We would like to express our gratitude to Zezheng Li and Liyuan Geng for their valuable assistance with test data preprocessing. Their contributions helped facilitate the progress of this work.

REFERENCES

- [1] S. Garg, T. Fischer, and M. Milford, “Where is your place, visual place recognition?” in *Proc. Int. Jt. Conf. Artif. Intell.*, vol. 8, 2021, pp. 4416–4425. 1
- [2] C. Masone and B. Caputo, “A survey on deep visual place recognition,” *IEEE Access*, vol. 9, pp. 19 516–19 547, 2021. 1, 2
- [3] A.-D. Doan, Y. Latif, T.-J. Chin, Y. Liu, T.-T. Do, and I. Reid, “Scalable place recognition under appearance change for autonomous driving,” in *Proc. IEEE/CVF Int. Conf. Comput. Vis.*, 2019, pp. 9319–9328. 1
- [4] P. Yin, L. Xu, X. Li, C. Yin, Y. Li, R. A. Srivatsan, L. Li, J. Ji, and Y. He, “A multi-domain feature learning method for visual place recognition,” in *Proc. IEEE Int. Conf. Robot. Automat.* IEEE, 2019, pp. 319–324. 1
- [5] Z. Xin, Y. Cai, T. Lu, X. Xing, S. Cai, J. Zhang, Y. Yang, and Y. Wang, “Localizing discriminative visual landmarks for place recognition,” in *Proc. IEEE Int. Conf. Robot. Automat.* IEEE, 2019, pp. 5979–5985. 1
- [6] A. Kornilova, I. Moskalenko, T. Pushkin, F. Tojiboev, R. Tariverdizadeh, and G. Ferrer, “Dominating set database selection for visual place recognition,” in *Proc. 21st Int. Conf. Adv. Robot.* IEEE, 2023, pp. 473–479. 1

- [7] G. Berton, C. Masone, and B. Caputo, "Rethinking visual geo-localization for large-scale applications," in *Proc. IEEE/CVF Conf. Comput. Vis. Pattern Recognit.*, 2022, pp. 4878–4888. 1, 4
- [8] R. Arandjelovic, P. Gronat, A. Torii, T. Pajdla, and J. Sivic, "Netvlad: Cnn architecture for weakly supervised place recognition," in *Proc. IEEE/CVF Int. Conf. Comput. Vis.*, 2016, pp. 5297–5307. 1, 2, 3, 4
- [9] A. Ali-Bey, B. Chaib-Draa, and P. Giguere, "Mixvpr: Feature mixing for visual place recognition," in *Proc. IEEE Winter Conf. Appl. Comput. Vis.*, 2023, pp. 2998–3007. 1, 2, 3, 4
- [10] N. Keetha, A. Mishra, J. Karhade, K. M. Jatavallabhula, S. Scherer, M. Krishna, and S. Garg, "Anyloc: Towards universal visual place recognition," *IEEE Robot. Automat. Lett.*, 2023. 1, 2, 4
- [11] S. Garg and M. Milford, "Fast, compact and highly scalable visual place recognition through sequence-based matching of overloaded representations," in *Proc. IEEE Int. Conf. Robot. Automat.* IEEE, 2020, pp. 3341–3348. 1, 2
- [12] M.-A. Tomita, B. Ferrarini, M. Milford, K. McDonald-Maier, and S. Ehsan, "Visual place recognition with low-resolution images," 2023. 1, 2
- [13] A. Oliva and A. Torralba, "Modeling the shape of the scene: A holistic representation of the spatial envelope," *Int. J. Comput. Vis.*, vol. 42, pp. 145–175, 2001. 2
- [14] N. Dalal and B. Triggs, "Histograms of oriented gradients for human detection," in *Proc. IEEE Comput. Soc. Conf. Comput. Vis. Pattern Recognit.*, vol. 1, 2005, pp. 886–893 vol. 1. 2
- [15] H. Jégou, M. Douze, C. Schmid, and P. Pérez, "Aggregating local descriptors into a compact image representation," in *Proc. IEEE Comput. Soc. Conf. Comput. Vis. Pattern Recognit.* IEEE, 2010, pp. 3304–3311. 2
- [16] S. Hausler, S. Garg, M. Xu, M. Milford, and T. Fischer, "Patchnetvlad: Multi-scale fusion of locally-global descriptors for place recognition," in *Proc. IEEE/CVF Conf. Comput. Vis. Pattern Recognit.*, 2021, pp. 14 141–14 152. 2, 4
- [17] S. Izquierdo and J. Civera, "Optimal transport aggregation for visual place recognition," in *Proc. IEEE/CVF Conf. Comput. Vis. Pattern Recognit.*, June 2024. 2, 4
- [18] A. Ali-bey, B. Chaib-draa, and P. Giguère, "Boq: A place is worth a bag of learnable queries," in *Proc. IEEE/CVF Conf. Comput. Vis. Pattern Recognit.*, 2024, pp. 17 794–17 803. 2
- [19] F. Lu, X. Lan, L. Zhang, D. Jiang, Y. Wang, and C. Yuan, "Cricavpr: Cross-image correlation-aware representation learning for visual place recognition," in *Proc. IEEE/CVF Conf. Comput. Vis. Pattern Recognit.*, June 2024. 2, 4
- [20] B. Ferrarini, M. J. Milford, K. D. McDonald-Maier, and S. Ehsan, "Binary neural networks for memory-efficient and effective visual place recognition in changing environments," *IEEE Trans. Robot.*, vol. 38, no. 4, pp. 2617–2631, 2022. 2
- [21] B. Arcanjo, B. Ferrarini, M. Milford, K. D. McDonald-Maier, and S. Ehsan, "An efficient and scalable collection of fly-inspired voting units for visual place recognition in changing environments," *IEEE Robot. Automat. Lett.*, vol. 7, no. 2, pp. 2527–2534, 2022. 2
- [22] A. Yang, M. Beheshti, T. E. Hudson, R. Vedanthan, W. Riewpaiboon, P. Mongkolwat, C. Feng, and J.-R. Rizzo, "Unav: An infrastructure-independent vision-based navigation system for people with blindness and low vision," *Sensors*, vol. 22, no. 22, p. 8894, 2022. 2
- [23] S. Zahedian, K. F. Sadabadi, and A. Nohekhan, "Localization of autonomous vehicles: Proof of concept for a computer vision approach," 2021. 2
- [24] M.-A. Tomita, B. Ferrarini, M. Milford, K. McDonald-Maier, and S. Ehsan, "Data efficient visual place recognition using extremely jpeg-compressed images," 2023. 2
- [25] A. Torii, J. Sivic, T. Pajdla, and M. Okutomi, "Visual place recognition with repetitive structures," in *Proc. IEEE/CVF Int. Conf. Comput. Vis.*, 2013, pp. 883–890. 2, 7
- [26] N. Sünderhauf, P. Neubert, and P. Protzel, "Are we there yet? challenging seqslam on a 3000 km journey across all four seasons," *Proc. of Workshop on Long-Term Autonomy, IEEE Int. Conf. Robot. Automat.*, p. 2013, 01 2013. 2, 3
- [27] F. Walch, C. Hazirbas, L. Leal-Taixé, T. Sattler, S. Hilsenbeck, and D. Cremers, "Image-based localization using lstms for structured feature correlation," in *Proc. IEEE/CVF Int. Conf. Comput. Vis.*, October 2017. 2, 6
- [28] A. Torii, R. Arandjelović, J. Sivic, M. Okutomi, and T. Pajdla, "24/7 place recognition by view synthesis," *IEEE Trans. Pattern Anal. Mach. Intell.*, vol. 40, no. 2, pp. 257–271, 2018. 2, 3
- [29] F. Warburg, S. Hauberg, M. Lopez-Antequera, P. Gargallo, Y. Kuang, and J. Civera, "Mapillary street-level sequences: A dataset for lifelong place recognition," in *Proc. IEEE/CVF Conf. Comput. Vis. Pattern Recognit.*, June 2020. 2, 3
- [30] D. Lee, S. Ryu, S. Yeon, Y. Lee, D. Kim, C. Han, Y. Cabon, P. Weinzaepfel, N. Guérin, G. Csurka, *et al.*, "Large-scale localization datasets in crowded indoor spaces," in *Proc. IEEE/CVF Conf. Comput. Vis. Pattern Recognit.*, 2021, pp. 3227–3236. 2, 6
- [31] D. Sheng, Y. Chai, X. Li, C. Feng, J. Lin, C. Silva, and J.-R. Rizzo, "Nyu-vpr: long-term visual place recognition benchmark with view direction and data anonymization influences," in *IEEE/RSJ Int. Conf. Intell. Robots Syst.* IEEE, 2021, pp. 9773–9779. 2, 6
- [32] A. Ali-bey, B. Chaib-draa, and P. Giguère, "Gsv-cities: Toward appropriate supervised visual place recognition," *Neurocomputing*, vol. 513, pp. 194–203, 2022. 2, 3
- [33] D. Sheng, A. Yang, J.-R. Rizzo, and C. Feng, "Nyc-indoor-vpr: A long-term indoor visual place recognition dataset with semi-automatic annotation," in *Proc. IEEE Int. Conf. Robot. Automat.*, 2024, pp. 14 853–14 859. 2, 6
- [34] G. Hudson, A. Léger, B. Niss, I. Sebestyen, and J. Vaaben, "Jpeg-1 standard 25 years: Past, present, and future reasons for a success," *Journal of Electronic Imaging*, vol. 27, p. 1, 08 2018. 2
- [35] M.-A. Tomita, B. Ferrarini, M. Milford, K. D. McDonald-Maier, and S. Ehsan, "Data-efficient sequence-based visual place recognition with highly compressed jpeg images," *ArXiv*, vol. abs/2302.13314, 2023. 2, 3
- [36] H. Carson, J. J. Ford, and M. Milford, "Unsupervised quality prediction for improved single-frame and weighted sequential visual place recognition," in *Proc. IEEE Int. Conf. Robot. Automat.*, 2023, pp. 3955–3961. 2
- [37] G. Hinton, O. Vinyals, and J. Dean, "Distilling the knowledge in a neural network," 2015. 2
- [38] Z. Hui, X. Wang, and X. Gao, "Fast and accurate single image super-resolution via information distillation network," in *Proc. IEEE/CVF Int. Conf. Comput. Vis.*, 2018, pp. 723–731. 2
- [39] F. Tung and G. Mori, "Similarity-preserving knowledge distillation," in *Proc. IEEE/CVF Int. Conf. Comput. Vis.*, 2019, pp. 1365–1374. 2
- [40] L. Liu, Q. Huang, S. Lin, H. Xie, B. Wang, X. Chang, and X. Liang, "Exploring inter-channel correlation for diversity-preserved knowledge distillation," in *Proc. IEEE/CVF Int. Conf. Comput. Vis.*, 2021, pp. 8271–8280. 2
- [41] Y. Shen, S. Zhou, J. Fu, R. Wang, S. Chen, and N. Zheng, "Structvpr: Distill structural knowledge with weighting samples for visual place recognition," in *Proc. IEEE/CVF Conf. Comput. Vis. Pattern Recognit.*, 2023, pp. 11 217–11 226. 2
- [42] C. Blakeney, X. Li, Y. Yan, and Z. Zong, "Craft distillation: Layer-wise convolutional neural network distillation," in *7th IEEE Int. Conf. Cyber Secur. Cloud Comput./6th IEEE Int. Conf. Edge Comput. Scalable Cloud*, 2020, pp. 252–257. 3
- [43] G. Berton, R. Mereu, G. Trivigno, C. Masone, G. Csurka, T. Sattler, and B. Caputo, "Deep visual geo-localization benchmark," in *Proc. IEEE/CVF Conf. Comput. Vis. Pattern Recognit.*, June 2022. 3
- [44] M. Oquab, T. Darcet, T. Moutakanni, H. V., M. Szafraniec, V. Khalidov, P. Fernandez, D. HAZIZA, F. Massa, A. El-Nouby, *et al.*, "DINOv2: Learning robust visual features without supervision," *Trans. Mach. Learn. Res.*, 2024. 4